

QuIP#: Even Better LLM Quantization with Hadamard Incoherence and Lattice Codebooks

Albert Tseng^{*1} Jerry Chee^{*1} Qingyao Sun² Volodymyr Kuleshov¹ Christopher De Sa¹

Abstract

Post-training quantization (PTQ) reduces the memory footprint of LLMs by quantizing their weights to low-precision. In this work, we introduce QuIP#, a weight-only PTQ method that achieves state-of-the-art results in extreme compression regimes (≤ 4 bits per weight) using three novel techniques. First, QuIP# improves the incoherence processing from QuIP (Chee et al., 2023) by using the randomized Hadamard transform, which is faster and has better theoretical properties. Second, QuIP# uses vector quantization techniques to take advantage of the ball-shaped sub-Gaussian distribution that incoherent weights possess: specifically, we introduce a set of hardware-efficient codebooks based on the highly symmetric E_8 lattice, which achieves the optimal 8-dimension unit ball packing. Third, QuIP# uses fine-tuning to improve fidelity to the original model. Our experiments show that QuIP# outperforms existing PTQ methods, enables new behaviors in PTQ scaling, and supports fast inference.

1. Introduction

Large language models (LLMs) have driven rapid advances across diverse fields such as natural language processing (Touvron et al., 2023b), scientific modeling (Nguyen et al., 2023), and program synthesis (Rozière et al., 2024). However, the massive size of these models poses significant challenges to their deployment. For example, the largest model in the Llama2 family has 70B parameters, and requires 140GB of GPU memory in native 16-bit precision (Touvron et al., 2023b). This massive memory footprint motivates research into methods that can compress LLMs without sacrificing quality.

^{*}Equal contribution ¹Department of Computer Science, Cornell University ²Department of Operations Research and Information Engineering, Cornell University. Correspondence to: Albert Tseng <albert@cs.cornell.edu>, Jerry Chee <jerrychee@cs.cornell.edu>, Code: <<https://github.com/Cornell-RelaxML/quip-sharp>>.

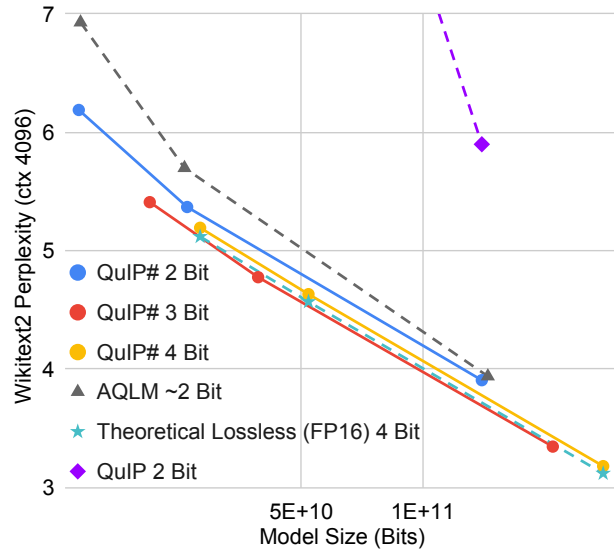


Figure 1. QuIP# offers unprecedented quantization quality at extreme compression ratios. QuIP# 3-bit models also scale better than theoretically lossless 4-bit models, a previously unseen result.

Post-training quantization (PTQ) reduces the memory requirements of large models by converting trained weights to a lower precision. For example, with 2-bit quantization, a 16-bit Llama2 model with 70B parameters fits on a single consumer-grade 24GB GPU and benefits from increased inference throughput (Cai et al., 2024). However, 2-bit quantization also often reduces the quality of the model and pushes the limits of PTQ algorithms (Chee et al., 2023).

In this work, we introduce QuIP#, a *weight-only* PTQ method that achieves a new state-of-the-art in model quantization. QuIP# improves over existing work via three techniques: incoherence processing, lattice codebooks, and fine-tuning. Incoherence processing is a principled form of outlier suppression that produces approximately sub-Gaussian distributed weight matrices (Chee et al., 2023). QuIP# performs incoherence processing with the computationally-efficient randomized Hadamard transform (Halko et al., 2011) (Section 3). To quantize incoherent matrices, QuIP# uses the BlockLDLQ block adaptive rounding algorithm with compressible codebooks based on the E_8 lattice, which

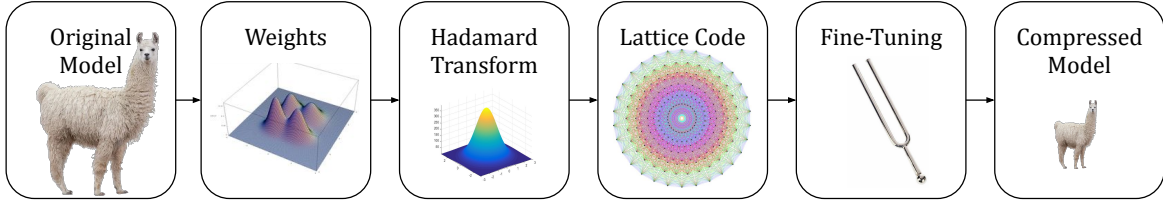


Figure 2. QuIP# performs incoherence processing with a Randomized Hadamard Transform and uses lattice codebooks to achieve state-of-the-art quantized models.

achieves the highest density 8 dimensional unit-ball packing (Viazovska, 2017) (Section 4). The E_8 lattice is highly structured and symmetric, which means that our codebooks are hardware-friendly and admit fast inference. Finally, QuIP# includes an inter-layer fine-tuning algorithm that further improves quantization quality (Section 5).

These developments allow QuIP# to significantly outperform existing PTQ methods including OmniQuant (Shao et al., 2024), QuIP (Chee et al., 2023) (a previous, separate work), and AQLM (Egiazarian et al., 2024). To the best of our knowledge, QuIP# is also the first PTQ method where 3-bit models scale better than 4-bit models. This directly refutes Dettmers & Zettlemoyer (2023)’s claim that 4-bit models are “optimal” and indicates that as the field of PTQ develops, 2-bit models are likely to scale better than 3-bit models in the near future.

Finally, we note that QuIP# was designed from the ground up to be fast. Algorithm 2 describes fast inference with a QuIP#-quantized linear layer. Our “proof of concept” CUDA implementation of QuIP# achieves over 50% of peak memory bandwidth on a NVIDIA RTX 4090, validating our design choices.

In summary, we introduce QuIP#, a post-training quantization method that achieves state-of-the-art results by

1. Performing incoherence processing with the Randomized Hadamard Transform, which has better incoherence properties and faster runtime than the Kronecker factorization in QuIP.
2. Rounding incoherence-processed weight matrices with block adaptive rounding and codebooks based on the E_8 lattice, which achieves the highest 8-dimension unit ball packing density (kissing number).
3. Introducing an inter-layer fine-tuning algorithm that further improves quantization quality.

2. Background / Related Work

2.1. Compressing LLMs

A large body of work has focused on compressing LLMs, as doing so can directly benefit LLM inference at scale. Methods such as pruning, quantization aware training (QAT), and

Algorithm 1 QuIP# without Fine-Tuning (QuIP#-NoFT)

input Weight $W \in \mathbb{R}^{m \times n}$, Hessians $H \in \mathbb{R}^{n \times n}$, g -dim. k -bit codebook C
 $\hat{W}, \hat{H}, S_U, S_V \leftarrow \text{IP-RHT}(W, H)$ (Alg. 3)
 $\hat{W} \leftarrow \text{BlockLDLQ}(\hat{W}, \hat{H}, C)$ (Sec. 4.1)
output \hat{W}, S_U, S_V

Algorithm 2 QuIP# Inference (for a Linear Layer)

input \hat{W}, S_U, S_V from Alg. 1, g -dim. k -bit codebook C ,
input $x \in \mathbb{R}^n$.
 $y \leftarrow \text{Had}(S_V \odot x)$ where Had performs
an orthogonal Hadamard transform (Sec. 3)
 $y \leftarrow \text{decompress_multiply}(\hat{W}, C, y)$
 $y \leftarrow \text{Had}(S_U \odot y)$
output y

post-training quantization (PTQ) all focus on different areas of this problem and are not strictly orthogonal to each other. Pruning *removes* weights from models while preserving model quality and inference performance (Chee et al., 2022; Sun et al., 2023). QAT focuses on training models that are more “quantizable” but usually requires training models from scratch (Nagel et al., 2022). PTQ, which QuIP# falls under, instead quantizes *pre-trained* models. PTQ generally requires much less compute than QAT and achieve competitive performance (Chee et al., 2023; Frantar et al., 2023; Shao et al., 2024; Egiazarian et al., 2024). For the rest of this paper, we focus on the PTQ realm of LLM compression.

2.2. Quantization and Adaptive Rounding

In QuIP#, we follow existing state-of-the-art PTQ methods and round weights to minimize the per-layer proxy loss, as formalized by Nagel et al. (2020):

$$\ell(\hat{W}) = E_x \left[\|\hat{W} - W\|_x^2 \right] \tag{1}$$

$$= \text{tr} \left((\hat{W} - W) H (\hat{W} - W)^T \right). \tag{2}$$

Here, $W \in \mathbb{R}^{m \times n}$ is the original weight matrix in a linear layer, $\hat{W} \in \mathbb{R}^{m \times n}$ are the quantized weights, $x \in \mathbb{R}^n$ is an input vector drawn uniformly at random from a calibration

set, and $H = E_x[xx^T]$ is a proxy Hessian. This intra-layer formulation makes quantization tractable for LLMs. One way to minimize ℓ is to use adaptive rounding methods that iteratively round weight matrices by considering the current rounding error for that specific matrix. For example, the LDLQ¹ rounding algorithm iteratively rounds rows of model weights using linear feedback from quantization error of already rounded rows. LDLQ is optimal within the class of adaptive rounding methods with linear feedback and offers provably better error rates than nearest or stochastic rounding (Chee et al., 2023).

2.3. Incoherence Processing

Multiple works have observed that outliers in model activations and weights can hinder quantization quality, motivating methods that “suppress” outliers during quantization. For example, AWQ (Lin et al., 2023) scales model weights by information from activations and OmniQuant (Shao et al., 2024) uses simple learnable model-preserving transformations. However, these heuristic-based approaches tend to fail at lower bitrates.

Instead, in QuIP, Chee et al. (2023) proposed that *incoherence* is important for LLM quantization. Informally, incoherent matrices have concentrated entry magnitudes—ruling out outliers. In LLMs, incoherent weight and Hessian matrices mean that both the thing being rounded (weights) and important rounding directions (Hessians) are not too large in any coordinate. This enables quantization with *provably* bounded error.

Definition 2.1 (Chee et al. (2023)). A Hessian $H \in \mathbb{R}^{n \times n}$ is μ -incoherent if its eigendecomposition $H = Q\Lambda Q^T$ has

$$\max_{i,j} |Q_{ij}| = \max_{i,j} |e_i^T Q e_j| \leq \mu / \sqrt{n}.$$

A weight matrix $W \in \mathbb{R}^{m \times n}$ is μ -incoherent if

$$\max_{i,j} |W_{ij}| = \max_{i,j} |e_i^T W e_j| \leq \mu \|W\|_F / \sqrt{mn}.$$

To exploit incoherence, Chee et al. (2023) introduced *incoherence processing* as a part of their quantization method QuIP. QuIP’s incoherence processing works by conjugating W and H by structured random orthogonal matrices. Specifically, QuIP constructs orthogonal matrices $U \in \mathbb{R}^{m \times m}$ and $V \in \mathbb{R}^{n \times n}$ via a Kronecker product by drawing uniform random orthogonal matrices U_1, U_2 (of sizes about \sqrt{n}), V_1 , and V_2 (of sizes about \sqrt{m}) and setting $U = U_1 \otimes U_2$ and $V = V_1 \otimes V_2$. If we assign $\tilde{H} \leftarrow VHV^T$ and $\tilde{W} \leftarrow UWV^T$, \tilde{H} and \tilde{W} become $\tilde{O}(1)$ -incoherent with high probability (see their Lemma 5). Note that this transformation preserves the proxy objective, as

¹OPTQ(Frantar et al., 2023) and QuIP independently introduced alternative formulations of this rounding method, and QuIP showed them to be equivalent. LDLQ is the name given by QuIP.

Algorithm 3 Incoherence Processing with RHT (IP-RHT)

input $W \in \mathbb{R}^{m \times n}, H \in \mathbb{R}^{n \times n}$

Sample sign vectors $S_V \sim \mathcal{U}\{\pm 1\}^n, S_U \sim \mathcal{U}\{\pm 1\}^m$

$\hat{W} \leftarrow \text{Had}(\text{diag}(S_U)\text{Had}(\text{diag}(S_V)W^T)^T)$ where

Had is the Hadamard transform (sec. 3)

$\hat{H} \leftarrow \text{Had}(\text{diag}(S_V)\text{Had}(\text{diag}(S_U)H)^T)$

output $\hat{W}, \hat{H}, S_U, S_V$

$\text{tr}((UWV^T)(VHV^T)(VW^T U^T)) = \text{tr}(WHW^T)$. After quantizing the transformed weight matrix \tilde{W} using \tilde{H} , during inference, QuIP-quantized models transform model activations x with V and U^T to compute

$$U^T(\text{quantized}(\tilde{W})(Vx)) \approx U^T(\tilde{W}(Vx)) = Wx.$$

These structured orthogonal multiplies by a Kronecker product lead to a runtime overhead of $\Theta(n\sqrt{n} + m\sqrt{m})$, which is small relative to the $\Theta(mn)$ cost of the multiply by W .

Incoherence processing can be seen as a principled alternative to more complicated and heuristic methods for outlier suppression. Methods such as grouping require extra storage and can negatively impact performance. For example, using a 16 bit scale per group of 64 weights requires an extra 0.25 bits per weight. This increase is significant in extreme compression regimes, whereas incoherence processing allows more bits to be spent on actually quantizing model weights.

2.4. Vector Quantization

Prior PTQ works have focused on quantizing each scalar weight W_{ij} individually (Chee et al., 2023; Lin et al., 2023; Shao et al., 2024). However, this can be suboptimal as the resulting codebook has low density and ignores the shape of the source distribution. Vector quantization (VQ) (Gray, 1984) instead quantizes a group of d weights together by assigning them to a d dimensional vector from some codebook C . To effectively use VQ, C should resemble the shape of the source distribution of W and have high code density. To quantize $v \in \mathbb{R}^d$ to k bits per entry, C should have 2^{kd} entries. VQ becomes intractable when kd is large, such as for large k or d . We resolve this exponential dependency on d with our rounding method BlockLDLQ in Section 4.1.

3. Incoherence Processing with the Randomized Hadamard Transform

In this section, we propose a way of improving the incoherence processing of QuIP by replacing the 2-factor Kronecker product by a Randomized Hadamard Transformation (RHT) (Halko et al., 2011). This change yields three advantages: (1) the theoretical bound on the incoherence parameter μ is improved; (2) the asymptotic cost of multiply-

ing by the structured random orthogonal matrix is improved from $\Theta(n\sqrt{n})$ to $\Theta(n \log n)$; (3) the cost to multiply is further reduced by a constant factor, since a Hadamard matrix multiply can be performed without any floating-point multiplies as its entries are in $\{-1, +1\}$. Additionally, we show in Section 6.4 that this change by itself improves the perplexity of quantized LLMs.

Recall from section 2.3 that one way to efficiently perform incoherence processing is to conjugate W and H by structured random orthogonal matrices. QuIP# uses the RHT, which performs $x \rightarrow VSx$ where $V \in \mathbb{R}^{n \times n}$ is a Hadamard matrix, S is a random sign vector $\{\pm 1\}^n$, and $x \in \mathbb{R}^n$. The RHT can be computed in $O(n \log n)$ time with the Fast Walsh-Hadamard Transform (Fino & Algazi, 1976) when n is a power of 2. We will temporarily assume that all dimensions are powers of 2. Later in the section we will explain 2 methods for incoherence processing when the dimension is not a power of 2.

Lemma 3.1. *Let H be any positive semidefinite matrix on $\mathbb{R}^{n \times n}$ and W any weight matrix on $\mathbb{R}^{m \times n}$. Let $U \in \mathbb{R}^{m \times m}$ and $V \in \mathbb{R}^{n \times n}$ be orthogonal scaled Hadamard matrices. Let $S_U \in \mathbb{R}^{m \times m}$ and $S_V \in \mathbb{R}^{n \times n}$ be random diagonal matrices with independent diagonal elements drawn uniformly from $\{-1, +1\}$. Then for any $\delta > 0$, $V S_V H S_V V^T$ is μ_H -incoherent with probability at least $1 - \delta$, and $U S_U W S_V V^T$ is μ_W -incoherent with probability at least $1 - \delta$, where*

$$\mu_H = \sqrt{2 \log \left(\frac{2n^2}{\delta} \right)} \quad \text{and} \quad \mu_W = 2 \log \left(\frac{4mn}{\delta} \right).$$

In QuIP (Chee et al., 2023), the 2-factor Kronecker approach achieves $\mu_W^{Kron} = A^2 \log(4Cmn/\delta)^2$, where A and C are global constants independent of n and the number of factors. QuIP#’s RHT achieves superior incoherence via a log dependence on the matrix size rather than the Kronecker method’s log-squared dependence. All of QuIP’s theory analyzing the proxy loss in Eq. (1) still holds with the RHT, with the improved incoherence rates propagating through.

Now, what about dimensions n that are not powers of 2? In most cases, we can factorize $n = pq$ where that p is the largest power of 2 such that there exists a known Hadamard matrix of size q . This allows us to construct $V \in \mathbb{R}^{n \times n} = H_p \otimes H_q$ where H_p and H_q are size p and q Hadamard matrices, respectively. Then we can compute VSx in $O(q^2 p \log p)$ time, which is faster than the $O(n(p + q))$ time of QuIP’s 2-factor Kronecker approach when $p \gg q$. For example, Llama 2 70B has intermediate dimension $28672 = 1024 * 28$; $1024 \gg 28$. Algorithm 3 describes how to perform incoherence processing with the RHT. Doing so requires storing two sign vectors $S_U \in \{\pm 1\}^m$ and $S_V \in \{\pm 1\}^n$. Since $n, m \gg 1000$ for LLMs, S_U and S_V add less than 0.01 bits per weight.

While the Hadamard conjecture states that $\exists H_k \forall k, 4 \mid k$, finding such Hadamard matrices is still an open problem (Hedayat & Wallis, 1978). In cases when there does not exist a factorization $n = pq$ where $\exists H_p, H_q$, we present a Randomized Fast Fourier Transform (RFFT) incoherence processing algorithm with similar runtime and concentration properties as the RHT. At a high level, the RFFT performs incoherence processing with the Fast Fourier Transform (FFT) (Cochran et al., 1967) and a random complex phase. The RFFT only requires n to be even, which is much weaker than the RHT’s restrictions on n . The RFFT is also useful when there *does exist* a decomposition $n = pq$ but $p \not\gg q$, resulting in reduced speedups over an $\Theta(n\sqrt{n})$ algorithm. The FFT itself is also well supported on a wide variety of hardware, meaning that it may be easier to implement a fast RFFT when adapting QuIP# to new hardware. In practice, we find that the RFFT performs slightly worse than the RHT but still achieves strong results (Table 1). We describe the RFFT in detail in Section A.2 in the Appendix.

Table 1. RHT vs. RFFT incoherence processing using 2 Bit QuIP# (no FT). WikiText2 perplexity (\downarrow), context length 4096.

INCOHERENCE	2-7B	2-13B	2-70B
HADAMARD	8.22	6.06	4.16
FOURIER	8.30	6.08	4.17

4. BlockLDLQ and Lattice Codebooks

The proof of Lemma 3.1 tells us that the incoherence-processed weights follow a roughly ball-shaped sub-Gaussian distribution. However, rounding weights one at a time, as QuIP does with its LDLQ, ignores this shaping—producing a set of representable weight vectors that is shaped like a hypercube rather than a ball. Vector quantization (VQ) lets us shape codebooks to better match the source distribution. In Section 4.1, we introduce BlockLDLQ, which iteratively rounds blocks of weights with VQ. Within BlockLDLQ’s VQ step, QuIP# uses the 2 bit E8P codebook (Section 4.2). E8P is based on the E_8 lattice, which achieves the highest density unit ball packing in \mathbb{R}^8 (Viazovska, 2017). E8P achieves good shaping while admitting fast inference from only needing to lookup from a size 256 codebook.

4.1. Adaptive Rounding for Vector Quantization

Chee et al. (2023) formulated a class of adaptive rounding algorithms with linear feedback. These methods round columns one at a time with linear feedback a_k from the already rounded columns. Specifically, columns of a weight matrix $W \in \mathbb{R}^{m \times n}$ are iteratively rounded for $k = 1, 2, \dots, n$: $\hat{W}_k = \mathcal{Q}(W_k + (W_{:(k-1)} - \hat{W}_{:(k-1)})a_k)$, where W_k is the k -th column of W , $W_{:(k-1)}$ is the first $k - 1$ columns of W , \mathcal{Q} performs nearest or stochastic

rounding, and $a_k \in \mathbb{R}^{k-1}$. The resulting \hat{W} satisfies $\hat{W} = \mathcal{Q}(W + (W - \hat{W})U)$, where $U \in \mathbb{R}^{n \times n}$ is an upper triangular matrix whose columns are a_k and \mathcal{Q} acts elementwise.

The LDLQ algorithm sets U to be $L^T - I$ where $H = L^T D L$ is the LDL decomposition of the proxy Hessian H . From QuIP, we know that LDLQ is optimal within adaptive rounding methods with linear feedback when rounding to the integers. However, LDLQ does not work with vector quantization, which rounds multiple columns together.

We propose to extend LDLQ to support vector quantization. Given a block size g that evenly divides n , our block LDLQ is based on a novel g -block LDL decomposition $H = \mathbf{L}^T \mathbf{D} \mathbf{L}$, where \mathbf{L} is a unit block lower triangular matrix (among the n^2/g^2 $g \times g$ blocks of $L \in \mathbb{R}^{n \times n}$, the n/g diagonal blocks are all I and all blocks above the diagonal are 0), and \mathbf{D} is a block diagonal matrix.² As before, we set $U = \mathbf{L}^T - I$, and round W in a block-wise fashion via

$$\hat{W}_k = \mathbf{Q}(W_k + (W_{:(k-1)} - \hat{W}_{:(k-1)})\mathbf{A}_k),$$

where $\mathbf{A}_k \in \mathbb{R}^{n \times g}$ contains the $k - g + 1$ through k -th columns of U (the k th block), W_k similarly denotes the k th block of W , and \mathbf{Q} denotes a vector quantizer. As in the original QuIP paper, we can bound the error of this method.

Theorem 4.1. *Suppose that we round $W \in \mathbb{R}^{m \times n}$ using g -block LDLQ with Hessian H , producing \hat{W} . Suppose that H is μ -incoherent, and that we use a (possibly stochastic) vector quantizer \mathbf{Q} that satisfies $\mathbf{E}[(\mathbf{Q}(x) - x)(\mathbf{Q}(x) - x)^T] \preceq \sigma^2 I$ for any $x \in \mathbb{R}^g$. Then*

$$\mathbf{E}[\text{tr}((\hat{W} - W)H(\hat{W} - W)^T)] \leq \frac{gm\mu^2\sigma^2}{n} \text{tr}(H^{1/2})^2.$$

Observe that under the same conditions, just quantizing all blocks independently would yield $\mathbf{E}[\text{tr}((\hat{W} - W)H(\hat{W} - W)^T)] \leq gm\sigma^2 \text{tr}(H)$: this “improvement” from the trace of H to the square of the trace of its square root divided by n is the same factor achieved in the scalar case in QuIP.³

4.2. The E8P (“E8 Padded”) Codebook

BlockLDLQ relies on an internal vector quantization (VQ) step \mathbf{Q} that rounds a d -dimension (g in the previous section) vector to a codebook C . To effectively apply VQ, C should be shaped like the source distribution and have high packing density. One way to improve shaping is by increasing d . However, recall from Section 2.4 that to quantize a vector

²It is straightforward to produce the g -block LDL decomposition from the Cholesky decomposition of H .

³The original QuIP paper also included multiple other technical guarantees, including a bound that considers more rigorously the “real” case of finite-sized codebooks. While these results could also be generalized to the block-LDLQ case, we view this as not providing much insight relevant to QuIP# beyond Theorem 4.1, so (if desired) they are left as an exercise for the reader.

$v \in \mathbb{R}^d$ to k bits with VQ, C must have size $2^{kd} \times d$. Since the codebook size is exponential in both the vector dimension and bitrate, VQ quickly becomes intractable at high dimensions or bitrates.

For QuIP#, we propose a novel 2-bit 8 dimensional *E8P codebook*, which contains 2^{16} entries but only requires lookups into a 2^8 -entry table, with the remaining 8 bits being used to store signs and shifts. E8P bypasses the scaling issues of VQ by taking advantage of the structure and symmetries of the E_8 lattice on which it is based. The E_8 lattice is composed of all-integer or all-half-integer vectors in \mathbb{R}^8 whose sum is an even number, that is

$$E_8 = (\mathbb{Z}^8 \cup (\mathbb{Z}^8 + \frac{1}{2})) \cap \{x \mid \mathbf{1}^T x \text{ is even}\}.$$

The construction of the E8P codebook starts with an equivalent way to write E_8 via the \hat{D}_8 lattice, where $\hat{D}_8 = \{x \in \mathbb{Z}^8 + \frac{1}{2} \mid \mathbf{1}^T x \text{ is even}\}$ is the set of half-integer vectors with even parity: here, $E_8 = \hat{D}_8 \cup (\hat{D}_8 + \frac{1}{2})$. It follows that $(\hat{D}_8 - \frac{1}{4}) \cup (\hat{D}_8 + \frac{1}{4}) = E_8 + \frac{1}{4}$ is just a shifted copy of E_8 (keeping the same optimal packing density).

\hat{D}_8 has nice symmetry properties: flipping any (nonzero) even number of signs of an element in \hat{D}_8 , yields another distinct element in \hat{D}_8 . This means that if $|\hat{D}_8|$ denotes the set of elementwise absolute values of entries in \hat{D}_8 , then each element of \hat{D}_8 can be expressed (uniquely) as the elementwise product of an entry $s \in |\hat{D}_8|$ and a sign vector of appropriate parity. So, if we start from some “source codebook” of absolute entries $S \subset |\hat{D}_8|$, we can use the 128 possible odd- or even-parity sign flips to generate a subset of \hat{D}_8 . Each entry in S is either an odd or even number of flips away from an entry in \hat{D}_8 , but not both. Thus, given $s \in S$ and 7 out of the 8 sign flips, we can infer the last one from the parity of the 7 sign flips and s . This lets us use the following pattern to store a 16-bit codeword in $E_8 + \frac{1}{4}$: 8 bits for the entry in S , 7 bits for sign flips, and 1 bit to $\pm \frac{1}{4}$. This lets us decode a size 2^{16} codebook by looking up into only a size 2^8 codebook (S) and performing some operations. All that remains is how to choose S : we set S to be the 227 elements of $|\hat{D}_8|$ with norm $\leq \sqrt{10}$ plus 29 “padding” elements from $|\hat{D}_8|$ with norm $\sqrt{12}$ (see Section C.1). We call this ball-shaped 2^{16} -entry lattice codebook “E8P.”

Figure 3 plots the elementwise MSE of quantizing a standard multivariate Gaussian to various k bit codebooks. Each k -bit codebook consists of a d -dimensional base lattice intersected with a ball to reach 2^{kd} points. The E_8 -based codebooks achieve lower MSEs than all other presented codebooks, including those based on the D_4 lattice (the even-parity vectors in \mathbb{Z}^4), which achieves the kissing number in \mathbb{R}^4 . This figure illustrates the importance of dimension for vector quantization. Increasing the vector dimension decreases the error for the half integer grid, as the resulting codebook is closer in shape to the source distribution.

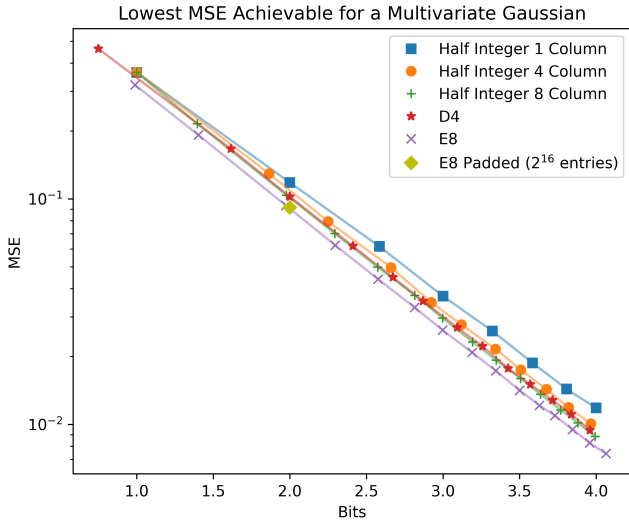


Figure 3. Minimum achievable elementwise MSE of quantizing a Gaussian to various codebooks. E_8 -based codebooks outperform other presented codebooks due to the underlying packing density and high dimensionality of E_8 .

Finally, while K-means on the source distribution would achieve lower MSE (Lloyd, 1982), there are a number of practical reasons why a K-means based codebook would be less practical, including worse end-to-end empirical performance. We discuss this more in Section C.3.

4.3. Scaling E_8 to Higher Bitrates

The E_8 lattice works well for low bitrates (e.g. 2 bits), but quickly becomes intractable at higher bitrates due to codebook size. In QuIP#, we use residual vector quantization (RVQ) (Juang & Gray, 1982) to get the benefits of lattice codebooks at higher bitrates. RVQ quantizes a vector x to p bits with a set q of q_i -bit codebooks (denoted $RVQ(x, p, q)$ where $p = \sum_{0 \leq i < |q|} q_i$) by repeatedly quantizing the quantization residual. That is, $RVQ(x, p, q) = \sum_{0 \leq i < |q|} \delta_i$ where $\delta_i = Q_{q_i} \left((x - \sum_{0 \leq j < i} \delta_j) / s_i \right) \cdot s_i$, we let $Q_{q_i}(\cdot)$ denote quantizing to a q_i bit codebook, and $s_i \in \mathbb{R}$. Using RVQ, we can quantize to 4 bits by rounding with the 2 bit E8P codebook twice. We can also quantize to 3 bits by using the 2 bit E8P codebook and a 1-bit E_8 codebook (elements of E_8 with norm ≤ 2 and 15 elements of E_8 with norm 4). One could also use more advanced multi-codebook quantization approaches other than RVQ, but we found that RVQ was sufficient to achieve strong quantization performance.

5. Fine-Tuning During Quantization

Recent works have suggested that at extreme quantization levels (e.g. 2 bits), inter-layer interactions are a significant hurdle to lossless quantization (Shao et al., 2024; Egiazarian et al., 2024). Here, we employ a simple fine-tuning algorithm that attempts to recover the original unquantized

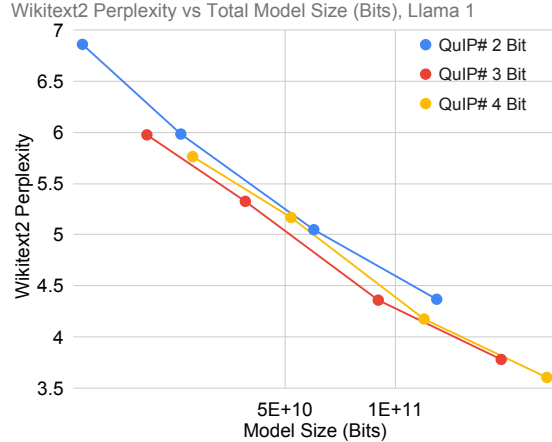


Figure 4. QuIP# scaling, Llama 1. Like Llama 2, QuIP# 3 bit scales better than QuIP# 4 bit for Llama 1 models and QuIP# 2 bit scales similarly to higher bitrates.

model during quantization. Our fine tuning method runs on a small development set and works by relaxing the sign vectors in the RHT to arbitrary real vectors *after quantization*.

Our fine tuning method contains two steps. First, we fine-tune within each transformer block by quantizing the first linear layer, fine-tuning the remaining parameters to match the unquantized model’s output activations on the unquantized model’s input activations, quantizing the second linear layer, fine-tuning, and so on until all linear layers are quantized. This step attempts to minimize the activation error caused by an individual linear layer *during quantization*, and it is parallelizable across transformer blocks as the activation error does not consider the effect of quantizing preceding blocks. The idea of fine-tuning on the level of a transformer block was previously proposed in Egiazarian et al. (2024); our methodology differs in that we set a different set of parameters to be trainable. In the second step, after all linear layers in the model are quantized, the unquantized parameters (layernorms, sign vectors, language model head) are fine-tuned to minimize activation error over the *entire model*.

By optimizing the sign vectors as real vectors instead of binary vectors in both steps, we allow the incoherence processing step to shape the weight matrix *to the codebook*. While this means we must store the sign vectors in FP16 instead of as bitvectors, the size of LLM matrices means that the sign vectors still add less than 0.01 bits per weight. We describe these steps in more detail in Section D.

6. Experiments

Our main experiments show the performance of QuIP# on the Llama 1 (Touvron et al., 2023a) and 2 (Touvron et al., 2023b) family of models. These models range in size from 7 billion to 70 billion parameters and offer good performance, making them suitable for understanding how quantization

Table 2. Llama 1 & 2 Wikitext2 and C4 perplexity (\downarrow), context length 2048.

METHOD	BITS	WIKITEXT 2							C4						
		1-7	1-13	1-30	1-65	2-7	2-13	2-70	1-7	1-13	1-30	1-65	2-7	2-13	2-70
FP16	16	5.68	5.09	4.10	3.53	5.47	4.88	3.32	7.08	6.61	5.98	5.62	6.97	6.47	5.52
AWQ	4	6.08	5.34	4.39	3.76	6.15	5.12	-	7.52	6.86	6.17	5.77	7.68	6.74	-
OMNIQ	4	5.86	5.21	4.25	3.71	5.74	5.02	3.47	7.34	6.76	6.11	5.73	7.35	6.65	5.65
QUIP# _{NO FT & NO E₈}	4	5.83	5.20	4.23	3.63	5.66	5.00	3.42	7.25	6.70	6.06	5.68	7.17	6.59	5.59
QUIP#	4	5.76	5.17	4.18	3.60	5.56	4.95	3.38	7.18	6.67	6.03	5.66	7.07	6.54	5.56
AWQ	3	11.9	7.45	10.0	5.21	24.0	10.5	-	13.3	9.13	12.7	7.11	23.9	13.1	-
OMNIQ	3	6.49	5.68	4.74	4.04	6.58	5.58	3.92	8.19	7.32	6.57	6.07	8.65	7.44	6.06
QUIP# _{NO FT & NO E₈}	3	6.29	5.52	4.54	3.91	6.19	5.34	3.71	7.82	6.98	6.29	5.86	7.85	6.98	5.78
QUIP#	3	5.98	5.31	4.36	3.78	5.79	5.10	3.56	7.39	6.83	6.17	5.77	7.32	6.72	5.67
OMNIQ	2	15.5	13.2	8.71	7.58	37.4	17.2	7.81	24.9	18.3	13.9	10.8	90.6	26.8	12.3
QUIP# _{NO FT & NO E₈}	2	9.95	7.18	5.80	5.02	12.3	7.60	4.87	11.7	8.67	7.55	6.83	14.8	9.57	6.82
QUIP#	2	6.86	5.97	5.02	4.36	6.66	5.74	4.16	8.36	7.48	6.71	6.19	8.35	7.45	6.12

Table 3. Zeroshot Accuracy (acc in LM Eval, not acc_norm), Llama 2.

METHOD	BITS	2-70					2-13					2-7				
		ARCC	ARCE	PIQA	WINO	ARCC	ARCE	PIQA	WINO	ARCC	ARCE	PIQA	WINO			
FP16	16	51.1	77.7	81.1	77.0	16	45.6	73.3	73.5	69.6	16	40.0	69.3	78.5	67.3	
OMNIQ	4	49.8	77.9	80.7	75.8	4	43.1	70.2	78.4	67.8	4	37.9	67.8	77.1	67.0	
QUIP	4	47.0	74.3	80.3	76.0	4	44.9	73.3	79.0	69.7	4	-	-	-	-	
AQLM	4.07	51.0	78.1	81.4	76.9	3.94	43.9	72.2	78.6	70.4	4.04	40.3	68.9	77.7	67.3	
QUIP#	4	50.6	78.1	81.4	77.1	4	45.5	73.9	78.9	69.9	4	40.5	69.1	78.4	67.6	
OMNIQ	3	47.6	75.7	79.7	73.5	3	42.0	69.0	77.7	65.9	3	35.3	62.6	73.6	63.6	
QUIP	3	46.3	73.2	80.0	74.6	3	41.5	70.4	76.9	69.9	3	-	-	-	-	
AQLM	3.01	50.0	77.6	81.3	77.2	3.03	43.6	73.5	77.8	67.6	3.04	38.7	67.8	76.6	68.4	
QUIP#	3	50.9	77.7	81.4	76.4	3	44.0	72.5	78.4	69.1	3	39.2	68.4	77.3	66.5	
OMNIQ	2	28.7	55.4	68.8	53.2	2	23.0	44.4	62.6	52.6	2	21.6	35.2	57.5	51.5	
QUIP	2	34.0	62.2	74.8	67.5	2	23.5	45.2	62.0	52.8	2	19.4	26.0	54.6	51.8	
AQLM	2.07	47.9	77.7	80.4	75.9	1.97	38.5	67.0	75.1	69.5	2.02	33.6	62.8	73.5	64.6	
QUIP#	2	48.7	77.3	80.3	75.9	2	39.5	69.3	77.3	67.7	2	34.6	64.6	75.1	64.9	

methods perform and scale. Additional results for other models are available in the Appendix.

In Section 6.1, we compare QuIP# with recently published weight-only PTQ methods. AWQ scales weights by activation magnitudes *before* quantizing to reduce outliers (Lin et al., 2023). OmniQuant learns model-preserving layerwise transformations that reduce outliers per transformer block (Shao et al., 2024). AQLM uses additive quantization with learnable per-layer codebooks and performs a fine-tuning step on codebook entries and layernorms (Egiazarian et al., 2024). We also include QuIP (Chee et al., 2023) as a baseline for the improvements in QuIP#.

We report $WxA16$ numbers for AWQ and OmniQuant from the OmniQuant paper and AQLM numbers from AQLM. We note that there are currently 2 methods for evaluating perplexity: using the Llama 1 context length of 2048 or using the model’s native context length (e.g. 4096 for Llama 2). OmniQuant and AWQ use 2048 for Llama 2 while AQLM uses 4096; we report both sets of numbers. We also note that AQLM paper reports QuIP# numbers from an outdated version of QuIP#. QuIP# is under active development and the numbers here represent the latest QuIP# numbers. Fi-

nally, we **bold** numbers in our tables when they are clearly better, such as a smaller model matching or outperforming a larger model or a similar sized model significantly outperforming another model.

6.1. QuIP# on Llama Models

Table 2 shows a comparison of QuIP# with OmniQuant, AWQ, and QuIP#(no FT and no lattice codebook E_8) with context length 2048. QuIP# offers a paradigm shift in quantization quality over OmniQuant and AWQ. Notably, while AWQ falls apart at even 2.15 bits (Shao et al., 2024) and OmniQuant produces unusable models at 2 bits, QuIP# produces high quality models that are close to OmniQuant 3 bit models. Table 2 also shows the importance of incoherence processing. QuIP# without fine-tuning or lattice codebooks significantly outperforms OmniQuant and AWQ, which both rely on heuristics to reduce model outliers during quantization.

Table 4 shows a comparison of QuIP# with AQLM with context length 4096. QuIP# offers strong improvements over AQLM at the 2 and 3 bit level, either significantly outperforming similarly sized models or offering similar per-

Table 4. Wikitext2 and C4 perplexity (\downarrow), context length 4096.

METHOD	2-7			2-13			2-70		
	BITS	W2	C4	BITS	W2	C4	BITS	W2	C4
FP16	16	5.12	6.63	16	4.57	6.05	16	3.12	4.97
QuIP#	4	5.19	6.75	4	4.63	6.13	4	3.18	5.02
↳ NO FT	4	5.22	6.79	4	4.65	6.15	4	3.18	5.02
↳ NO E_8	4	5.29	6.86	4	4.68	6.20	4	3.22	5.05
QuIP	4	-	-	4	4.76	6.29	4	3.58	5.38
AQLM	4.04	5.21	6.74	3.94	4.64	6.14	4.07	3.17	5.01
QuIP#	3	5.41	7.04	3	4.78	6.35	3	3.35	5.15
↳ NO FT	3	5.60	7.34	3	4.90	6.50	3	3.41	5.20
↳ NO E_8	3	5.77	7.61	3	4.99	6.65	3	3.48	5.28
QuIP	3	-	-	3	5.12	6.79	3	3.87	5.67
AQLM	3.04	5.46	7.10	3.03	4.83	6.37	3.01	3.36	5.17
QuIP#	2	6.19	8.16	2	5.35	7.20	2	3.91	5.71
↳ NO FT	2	8.22	11.0	2	6.06	8.07	2	4.16	6.01
↳ NO E_8	2	11.2	14.5	2	7.04	9.37	2	4.58	6.51
QuIP	2	-	-	2	13.5	16.2	2	5.90	8.17
AQLM	2.02	6.93	8.84	1.97	5.70	7.59	2.07	3.94	5.72

Table 5. 2 and 4 bit QuIP# Llama model generation speed measured on a NVIDIA RTX 4090 with a “proof of concept” CUDA implementation of E8P. QuIP# achieves > 50% peak memory bandwidth (1008GB/s) during generation and is fast and scalable.

MODEL	2 BIT	2 BIT %	4 BIT	4 BIT %
	TOK/S	MEM BW	TOK/S	MEM BW
2-7B	170.50	29.60%	117.73	40.87%
2-13B	104.83	33.80%	71.09	45.84%
1-30B	51.60	38.39%	32.50	48.36%
2-70B	32.74	56.84%	OOM	OOM

formance with a smaller model⁴. At the 4 bit level, QuIP# and AQLM both perform similarly. This is not surprising as state-of-the-art 4 bit models are all very close to FP16 performance. Furthermore, the QuIP# 3 and 4 bit results presented in this paper use residual vector quantization; one could potentially achieve better numbers with more advanced multi-codebook quantization approaches.

Table 3 shows zeroshot results for QuIP#, AQLM, and OmniQuant. Both AQLM and QuIP# significantly outperform OmniQuant, which correlates with the perplexity results. AQLM and QuIP# both perform very close to FP16 at higher bitrates and for larger models, but QuIP# tends to outperform AQLM at lower bitrates and model sizes. We note that zeroshot tasks have an element of randomness and even FP16 numbers can disagree by up to 0.5%.

6.2. QuIP# Bit Scaling

Figures 1 (first page) and 4 show how QuIP# scales on the Llama family of models and Wikitext2. On both Llama 1

⁴In our experience, at extreme quantization levels, even 0.1 bits can make a significant difference in quantization quality.

and 2, QuIP# 3 bit outperforms QuIP# 4 bit and QuIP# 2 bit offers similar scaling to 3 and 4 bit models. Furthermore, on Llama 2, QuIP# 3 bit outperforms a theoretical lossless 4 bit model (FP16 at 4 bits). To the best of our knowledge, this is the first time a 3 bit PTQ method has outperformed a theoretical lossless 4 bit model and also the first time a 2 bit PTQ method has offered similar scaling to higher bitrates.

6.3. Efficient Inference with QuIP#

Table 5 shows 2 and 4 bit QuIP# Llama model generation speed measured on a NVIDIA RTX 4090 GPU with a “proof of concept” CUDA implementation of E8P and the FlashAttention library (Dao et al., 2022; Dao, 2023) implementation of Llama. 4 bit generation speed is faster than 50% of the 2 bit speed since both bitrates still need to perform two Hadamard multiplies per linear layer. We note that we are not CUDA experts and a better optimized implementation of E8P could likely achieve higher throughput. Nevertheless, we find that QuIP# inference is fast and scalable on modern GPUs.

6.4. Ablations

Table 4 also contains an ablation on the various components of QuIP#. The “no FT” row shows QuIP# without fine-tuning and the “no E_8 ” row shows QuIP# without fine-tuning and lattice codebooks. For the latter, we round to the 1-dimensional half-integer grid. We also include QuIP numbers as reported by AQLM. At all bitrates, each component of QuIP# brings additional performance gains. The difference between QuIP and QuIP# without fine-tuning and lattice codebooks also shows the difference between QuIP’s Kronecker factorization and QuIP#’s RHT. The RHT offers stronger incoherence properties than the Kronecker factorization (Section 3), which improves performance.

7. Conclusion

We present QuIP#, a weight-only post training compression method that achieves state-of-the-art results on LLMs at 2, 3, and 4 bits per weight. QuIP# uses the Randomized Hadamard Transform as an efficient and principled form of outlier suppression, and introduces the E_8 lattice-based E8P codebook to better quantize RHT transformed weights. The E8P codebook is highly symmetric and admits fast inference, allowing a “proof of concept” QuIP# CUDA implementation to achieve over 50% peak memory bandwidth on modern GPUs. QuIP# also implements inter-layer fine tuning, further improving quantization. To the best of our knowledge, QuIP# is the first PTQ method to achieve superior scaling at 3 bits over 4 bits and similar scaling at 2 bits to higher bitrates. Our results indicate that, in the near future, 2 bit models are likely to scale better than 3 bit ones.

8. Impact Statement

This paper presents work whose goal is to advance the field of Machine Learning. There are many potential societal consequences of our work, none which we feel must be specifically highlighted here.

Acknowledgements

We thank, in no particular order, David Hou for helping with the QuIP# CUDA implementation, Tiancheng Yuan for lending his RTX 4090 and helping with acquiring QuIP# timing numbers, Tri Dao for a fast CUDA implementation of the Hadamard transform and general help with QuIP#, and Together AI for compute resources.

References

- Almazrouei, E., Alobeidli, H., Alshamsi, A., Cappelli, A., Cojocar, R., Debbah, M., Étienne Goffinet, Hesslow, D., Launay, J., Malartic, Q., Mazzotta, D., Noune, B., Pannier, B., and Penedo, G. The falcon series of open language models, 2023.
- Cai, T., Li, Y., Geng, Z., Peng, H., Lee, J. D., Chen, D., and Dao, T. Medusa: Simple llm inference acceleration framework with multiple decoding heads. *arXiv preprint arXiv: 2401.10774*, 2024.
- Chee, J., Renz, M., Damle, A., and Sa, C. D. Model preserving compression for neural networks. In Oh, A. H., Agarwal, A., Belgrave, D., and Cho, K. (eds.), *Advances in Neural Information Processing Systems*, 2022. URL <https://openreview.net/forum?id=gt-l9Hu2ndd>.
- Chee, J., Cai, Y., Kuleshov, V., and Sa, C. D. QuIP: 2-bit quantization of large language models with guarantees. In *Thirty-seventh Conference on Neural Information Processing Systems*, 2023. URL <https://openreview.net/forum?id=xrk9g5vcXR>.
- Cochran, W., Cooley, J., Favon, D., Helms, H., Kaenel, R., Lang, W., Maling, G., Nelson, D., Rader, C., and Welch, P. What is the fast fourier transform? *Proceedings of the IEEE*, 55(10):1664–1674, 1967. doi: 10.1109/PROC.1967.5957.
- Computer, T. Redpajama: An open source recipe to reproduce llama training dataset, 2023. URL <https://github.com/togethercomputer/RedPajama-Data>.
- Dao, T. FlashAttention-2: Faster attention with better parallelism and work partitioning. 2023.
- Dao, T., Fu, D. Y., Ermon, S., Rudra, A., and Ré, C. FlashAttention: Fast and memory-efficient exact attention with IO-awareness. In *Advances in Neural Information Processing Systems*, 2022.
- Dettmers, T. and Zettlemoyer, L. The case for 4-bit precision: k-bit inference scaling laws. In Krause, A., Brunskill, E., Cho, K., Engelhardt, B., Sabato, S., and Scarlett, J. (eds.), *Proceedings of the 40th International Conference on Machine Learning*, volume 202 of *Proceedings of Machine Learning Research*, pp. 7750–7774. PMLR, 23–29 Jul 2023. URL <https://proceedings.mlr.press/v202/dettmers23a.html>.
- Egiazarian, V., Panferov, A., Kuznedev, D., Frantar, E., Babenko, A., and Alistarh, D. Extreme compression of large language models via additive quantization, 2024.
- Fino and Algazi. Unified matrix treatment of the fast walsh-hadamard transform. *IEEE Transactions on Computers*, C-25(11):1142–1146, 1976. doi: 10.1109/TC.1976.1674569.
- Frantar, E., Ashkboos, S., Hoefler, T., and Alistarh, D. OPTQ: Accurate quantization for generative pre-trained transformers. In *The Eleventh International Conference on Learning Representations*, 2023. URL <https://openreview.net/forum?id=tcbBPnfwxS>.
- Gao, L., Tow, J., Abbasi, B., Biderman, S., Black, S., DiPofi, A., Foster, C., Golding, L., Hsu, J., Le Noac’h, A., Li, H., McDonnell, K., Muennighoff, N., Ociepa, C., Phang, J., Reynolds, L., Schoelkopf, H., Skowron, A., Sutawika, L., Tang, E., Thite, A., Wang, B., Wang, K., and Zou, A. A framework for few-shot language model evaluation, 12 2023. URL <https://zenodo.org/records/10256836>.
- Gray, R. Vector quantization. *IEEE ASSP Magazine*, 1(2): 4–29, 1984. doi: 10.1109/MASSP.1984.1162229.
- Halko, N., Martinsson, P.-G., and Tropp, J. A. Finding structure with randomness: Probabilistic algorithms for constructing approximate matrix decompositions. *SIAM review*, 53(2):217–288, 2011.
- Hedayat, A. and Wallis, W. D. Hadamard Matrices and Their Applications. *The Annals of Statistics*, 6(6):1184 – 1238, 1978. doi: 10.1214/aos/1176344370. URL <https://doi.org/10.1214/aos/1176344370>.
- Jiang, A. Q., Sablayrolles, A., Roux, A., Mensch, A., Savary, B., Bamford, C., Chaplot, D. S., de las Casas, D., Hanna, E. B., Bressand, F., Lengyel, G., Bour, G., Lample, G., Lavaud, L. R., Saulnier, L., Lachaux, M.-A., Stock, P., Subramanian, S., Yang, S., Antoniak, S., Scao, T. L., Gervet, T., Lavril, T., Wang, T., Lacroix, T., and Sayed, W. E. Mixtral of experts, 2024.

- Juang, B.-H. and Gray, A. Multiple stage vector quantization for speech coding. In *ICASSP '82. IEEE International Conference on Acoustics, Speech, and Signal Processing*, volume 7, pp. 597–600, 1982. doi: 10.1109/ICASSP.1982.1171604.
- Kingma, D. P. and Ba, J. Adam: A method for stochastic optimization, 2017.
- Lin, J., Tang, J., Tang, H., Yang, S., Dang, X., Gan, C., and Han, S. Awq: Activation-aware weight quantization for llm compression and acceleration, 2023.
- Lloyd, S. Least squares quantization in pcm. *IEEE Transactions on Information Theory*, 28(2):129–137, 1982. doi: 10.1109/TIT.1982.1056489.
- Nagel, M., Amjad, R. A., Van Baalen, M., Louizos, C., and Blankevoort, T. Up or down? Adaptive rounding for post-training quantization. In III, H. D. and Singh, A. (eds.), *Proceedings of the 37th International Conference on Machine Learning*, volume 119 of *Proceedings of Machine Learning Research*, pp. 7197–7206. PMLR, 13–18 Jul 2020. URL <https://proceedings.mlr.press/v119/nagel20a.html>.
- Nagel, M., Fournarakis, M., Bondarenko, Y., and Blankevoort, T. Overcoming oscillations in quantization-aware training. In Chaudhuri, K., Jegelka, S., Song, L., Szepesvari, C., Niu, G., and Sabato, S. (eds.), *Proceedings of the 39th International Conference on Machine Learning*, volume 162 of *Proceedings of Machine Learning Research*, pp. 16318–16330. PMLR, 17–23 Jul 2022. URL <https://proceedings.mlr.press/v162/nagel22a.html>.
- Nguyen, E., Poli, M., Faizi, M., Thomas, A., Birch-Sykes, C., Wornow, M., Patel, A., Rabideau, C., Massaroli, S., Bengio, Y., Ermon, S., Baccus, S. A., and Ré, C. Hye-nadna: Long-range genomic sequence modeling at single nucleotide resolution. 2023.
- Rozière, B., Gehring, J., Gloeckle, F., Sootla, S., Gat, I., Tan, X. E., Adi, Y., Liu, J., Sauvestre, R., Remez, T., Rapin, J., Kozhevnikov, A., Evtimov, I., Bitton, J., Bhatt, M., Ferrer, C. C., Grattafiori, A., Xiong, W., Défossez, A., Copet, J., Azhar, F., Touvron, H., Martin, L., Usunier, N., Scialom, T., and Synnaeve, G. Code llama: Open foundation models for code, 2024.
- Shao, W., Chen, M., Zhang, Z., Xu, P., Zhao, L., Li, Z., Zhang, K., Gao, P., Qiao, Y., and Luo, P. Omniquant: Omnidirectionally calibrated quantization for large language models. In *The Twelfth International Conference on Learning Representations*, 2024. URL <https://openreview.net/forum?id=8Wuvvh0LYW>.
- Sloane, N. Hadamard Matrices — neilsloane.com. <http://neilsloane.com/hadamard/>. [Accessed 02-02-2024].
- Sun, M., Liu, Z., Bair, A., and Kolter, J. Z. A simple and effective pruning approach for large language models. In *Workshop on Efficient Systems for Foundation Models @ ICML2023*, 2023. URL <https://openreview.net/forum?id=tz9JV2PRsv>.
- Touvron, H., Lavril, T., Izacard, G., Martinet, X., Lachaux, M.-A., Lacroix, T., Rozière, B., Goyal, N., Hambro, E., Azhar, F., Rodriguez, A., Joulin, A., Grave, E., and Lample, G. Llama: Open and efficient foundation language models, 2023a.
- Touvron, H., Martin, L., Stone, K., Albert, P., Almahairi, A., Babaei, Y., Bashlykov, N., Batra, S., Bhargava, P., Bhosale, S., Bikel, D., Blecher, L., Ferrer, C. C., Chen, M., Cucurull, G., Esiobu, D., Fernandes, J., Fu, J., Fu, W., Fuller, B., Gao, C., Goswami, V., Goyal, N., Hartshorn, A., Hosseini, S., Hou, R., Inan, H., Kardas, M., Kerkez, V., Khabsa, M., Kloumann, I., Korenev, A., Koura, P. S., Lachaux, M.-A., Lavril, T., Lee, J., Liskovich, D., Lu, Y., Mao, Y., Martinet, X., Mihaylov, T., Mishra, P., Molybog, I., Nie, Y., Poulton, A., Reizenstein, J., Rungta, R., Saladi, K., Schelten, A., Silva, R., Smith, E. M., Subramanian, R., Tan, X. E., Tang, B., Taylor, R., Williams, A., Kuan, J. X., Xu, P., Yan, Z., Zarov, I., Zhang, Y., Fan, A., Kambadur, M., Narang, S., Rodriguez, A., Stojnic, R., Edunov, S., and Scialom, T. Llama 2: Open foundation and fine-tuned chat models, 2023b.
- Viazovska, M. The sphere packing problem in dimension 8. *Annals of Mathematics*, 185(3), May 2017. ISSN 0003-486X. doi: 10.4007/annals.2017.185.3.7. URL <http://dx.doi.org/10.4007/annals.2017.185.3.7>.

A. Concentration Inequalities for the Randomized Hadamard Transform and Fast Fourier Transform

A.1. Incoherence Processing with the Randomized Hadamard Transform

Lemma A.1. *For any non-negative real number n ,*

$$\frac{1}{B(n, 1/2)} \int_{-1}^{+1} (1-x^2)^{n-1} \cdot \exp(tx) dx \leq \exp\left(\frac{t^2}{4n+2}\right).$$

Proof. We start with the following “standard” integral. For non-negative integer m and real $n > 0$,

$$\int_{-1}^{+1} x^{2m}(1-x^2)^{n-1} dx = B\left(m + \frac{1}{2}, n\right) = \frac{\Gamma\left(m + \frac{1}{2}\right) \Gamma(n)}{\Gamma\left(m + n + \frac{1}{2}\right)}.$$

This means that

$$\begin{aligned} \frac{1}{B\left(\frac{1}{2}, n\right)} \int_{-1}^{+1} x^{2m}(1-x^2)^{n-1} dx &= \frac{B\left(m + \frac{1}{2}, n\right)}{B\left(\frac{1}{2}, n\right)} \\ &= \frac{\Gamma\left(m + \frac{1}{2}\right) \Gamma(n)}{\Gamma\left(m + n + \frac{1}{2}\right)} \cdot \frac{\Gamma\left(n + \frac{1}{2}\right)}{\Gamma\left(\frac{1}{2}\right) \Gamma(n)} \\ &= \frac{\Gamma\left(m + \frac{1}{2}\right) \Gamma\left(n + \frac{1}{2}\right)}{\sqrt{\pi} \cdot \Gamma\left(m + n + \frac{1}{2}\right)}. \end{aligned}$$

Applying the Legendre duplication formula, for integer m ,

$$\Gamma\left(m + \frac{1}{2}\right) = \frac{(2m)! \sqrt{\pi}}{4^m m!},$$

then

$$\begin{aligned} \frac{1}{B\left(\frac{1}{2}, n\right)} \int_{-1}^{+1} x^{2m}(1-x^2)^{n-1} dx &= \frac{(2m)! \sqrt{\pi}}{4^m m!} \cdot \frac{(2n)! \sqrt{\pi}}{4^n n!} \cdot \frac{1}{\sqrt{\pi}} \cdot \frac{4^{m+n} (m+n)!}{(2m+2n)! \sqrt{\pi}} \\ &= \frac{(2m)! (2n)! (m+n)!}{m! n! (2m+2n)!}. \end{aligned}$$

In particular, this means that

$$\begin{aligned}
\frac{1}{B\left(\frac{1}{2}, n\right)} \int_{-1}^{+1} \exp(tx)(1-x^2)^{n-1} dx &= \sum_{m=0}^{\infty} \frac{t^{2m}}{(2m)!} \cdot \frac{1}{B\left(\frac{1}{2}, n\right)} \int_{-1}^{+1} x^{2m}(1-x^2)^{n-1} dx \\
&= \sum_{m=0}^{\infty} \frac{t^{2m}}{(2m)!} \cdot \frac{(2m)!(2n)!(m+n)!}{m!n!(2m+2n)!} \\
&= \sum_{m=0}^{\infty} \frac{t^{2m}}{m!} \cdot \frac{(2n)!(m+n)!}{n!(2m+2n)!} \\
&= \sum_{m=0}^{\infty} \frac{t^{2m}}{m!} \cdot \prod_{k=1}^m \frac{k+n}{(2k+2n)(2k+2n-1)} \\
&= \sum_{m=0}^{\infty} \frac{t^{2m}}{m!} \cdot \frac{1}{2^m} \prod_{k=1}^m \frac{1}{2k+2n-1} \\
&\leq \sum_{m=0}^{\infty} \frac{t^{2m}}{m!} \cdot \frac{1}{2^m} \left(\frac{1}{2n+1}\right)^m \\
&= \sum_{m=0}^{\infty} \frac{1}{m!} \left(\frac{t^2}{4n+2}\right)^m \\
&= \exp\left(\frac{t^2}{4n+2}\right).
\end{aligned}$$

This proves the lemma

$$\frac{1}{B(n, 1/2)} \int_{-1}^{+1} (1-x^2)^{n-1} \cdot \exp(tx) dx \leq \exp\left(\frac{t^2}{4n+2}\right).$$

□

Lemma A.2. Call $U \in \mathbb{R}^{nd \times nd}$ an (n, d) -block orthohadamard matrix if it has the following properties: (1) U is a orthogonal matrix, and (2) each aligned $d \times d$ block of U is $1/\sqrt{n}$ times an orthogonal matrix. This generalizes the notion of Hadamard matrices. Let $S \in \mathbb{R}^{nd \times nd}$ be a random block diagonal matrix, where each $d \times d$ block of the diagonal is sampled independently and uniformly from the set of (possibly special) orthogonal matrices. Then we call multiplication by US a randomized orthohadamard transform, and observe that it has the following nice property. Let $x \in \mathbb{R}^{nd}$ be any fixed vector, and let $b \in \mathbb{R}^{nd}$ be a fixed vector that is sparse in the sense that it is supported only on a single d -sized aligned block (i.e. all but one of the n blocks are zero). Then

$$\mathbf{P}(|b^T USx| \geq a) \leq 2 \exp\left(-\frac{a^2 nd}{2 \|b\|^2 \|x\|^2}\right).$$

Proof. If we let the i th block of x be $x_i \in \mathbb{R}^d$ and let the i th block of $S^T U^T b^T$ be v_i , then the v_i will be independent and uniformly distributed on the sphere in d dimensional space of radius $\|b\|/\sqrt{n}$, and so $v_i^T x_i = \|b\| \|x_i\| n^{-1/2} z_i$, where the z_i are all independent and distributed according to an entry of a random point on the unit sphere in d dimensional space. Observe that this means that

$$\mathbf{P}(z_i) \propto (1 - z_i^2)^{\frac{d-1}{2}-1}.$$

So,

$$\begin{aligned}
 \mathbf{E} [\exp (tb^T U S x)] &= \mathbf{E} \left[\exp \left(t \sum_{i=1}^n \|b\| \|x_i\| n^{-1/2} z_i \right) \right] \\
 &= \prod_{i=1}^n \mathbf{E} \left[\exp \left(t \|b\| \|x_i\| n^{-1/2} z_i \right) \right] \\
 &\leq \prod_{i=1}^n \mathbf{E} \left[\exp \left(\frac{1}{4 \cdot \frac{d-1}{2} + 2} \right) \left(t \|b\| \|x_i\| n^{-1/2} \right)^2 \right] \\
 &= \prod_{i=1}^n \mathbf{E} \left[\exp \left(\frac{t^2 \|b\|^2 \|x_i\|^2}{2nd} \right) \right] \\
 &= \mathbf{E} \left[\exp \left(\frac{t^2 \|b\|^2 \|x\|^2}{2nd} \right) \right],
 \end{aligned}$$

where the the last line follows from Lemma A.1. It follows from the standard application of Markov's inequality that for any $a > 0$,

$$\mathbf{P} (|b^T U S x| \geq a) \leq 2 \exp \left(-\frac{a^2 nd}{2 \|b\|^2 \|x\|^2} \right).$$

This is what we wanted to show. □

Lemma A.3. *Let $H \in \mathbb{R}^{n \times n}$ be an orthogonal scaled Hadamard matrix or $F \in \mathbb{R}^{n \times n}$ be an orthogonal FFT matrix (the FFT understood as operating on a real vector space). Let $S \in \mathbb{R}^{n \times n}$ be a random diagonal matrix with diagonal elements supported on \mathbb{R}^n , and let $P \in \mathbb{R}^{n \times n}$ be a random 2-block-diagonal matrix with 2×2 diagonal blocks supported on $\text{SO}(2)$ (we can also think of this as acting like a diagonal complex matrix with each diagonal element a random complex number of absolute value 1). Let $U \in \mathbb{R}^{n \times n}$ be any fixed orthogonal matrix. Then, for any $\epsilon > 0$,*

$$\text{Prob} \left(\max_{i,j} |e_i^T H S U e_j| \geq \sqrt{\frac{2}{nd} \log \left(\frac{2n^2}{\epsilon} \right)} \right) \leq \epsilon$$

and

$$\text{Prob} \left(\max_{i,j} |e_i^T F P U e_j| \geq \sqrt{\frac{2}{nd} \log \left(\frac{2n^2}{\epsilon} \right)} \right) \leq \epsilon.$$

That is, with probability at least $1 - \epsilon$, multiplying by either HS or FP makes the resulting orthogonal matrix μ -incoherent, where

$$\mu_H = \sqrt{2 \log \left(\frac{2n^2}{\epsilon} \right)}.$$

Proof. Setting $b = e_i$ and $x = U e_j$ in Lemma A.2,

$$\mathbf{P} (|e_i^T H S U e_j| \geq a) \leq 2 \exp \left(-\frac{a^2 nd}{2} \right).$$

By the union bound,

$$\mathbf{P} \left(\max_{i,j} |e_i^T H S U e_j| \geq a \right) \leq 2n^2 \exp \left(-\frac{a^2 nd}{2} \right).$$

Setting

$$a^2 = \frac{2}{nd} \log \left(\frac{2n^2}{\epsilon} \right)$$

proves the lemma. The FFT case is identical. □

Algorithm 4 Incoherence Processing with RFFT (IP-RFFT)

input $W \in \mathbb{R}^{m \times n}, H \in \mathbb{R}^{n \times n}$

Sample phase vectors

$$\theta_V \sim \mathcal{U}[0, 2\pi]^{n/2}, \theta_U \sim \mathcal{U}[0, 2\pi]^{m/2}$$

$$S_V = \cos(\theta_V) + i \sin(\theta_V), S_U = \cos(\theta_U) + i \sin(\theta_U)$$

$\hat{W} \leftarrow \text{FFT}(\text{diag}(S_U) \text{FFT}(\text{diag}(S_V) W^T)^T)$ where

FFT is the Fast Fourier transform (Sec. A.2)

$\hat{H} \leftarrow \text{FFT}(\text{diag}(S_V) \text{FFT}(\text{diag}(S_U) H)^T)$

output $\hat{W}, \hat{H}, S_U, S_V$

Lemma A.4. Let $H_L \in \mathbb{R}^{m \times m}$ be an orthogonal scaled Hadamard matrix or $F \in \mathbb{R}^{m \times m}$ be an orthogonal FFT matrix (the FFT understood as operating on a real vector space). Let $S_L \in \mathbb{R}^{m \times m}$ be a random diagonal matrix with diagonal elements supported on \mathbb{R}^m , and let $P \in \mathbb{R}^{m \times m}$ be a random 2-block-diagonal matrix with 2×2 diagonal blocks supported on $\text{SO}(2)$. Let $H_R \in \mathbb{R}^{n \times n}$, F_R , S_R , and P_R be defined analogously over n -dimensional space. Let $W \in \mathbb{R}^{m \times n}$ be any fixed matrix. Then, for any $\epsilon > 0$,

$$\mathbf{P} \left(\max_{i,j} |e_i^T H_L S_L W S_R^T H_R^T e_j| \geq \|W\|_F \sqrt{\frac{4}{mn}} \log \left(\frac{4mn}{\epsilon} \right) \right) \leq \epsilon.$$

and

$$\mathbf{P} \left(\max_{i,j} |e_i^T F_L P_L W P_R^T F_R^T e_j| \geq \|W\|_F \sqrt{\frac{4}{mn}} \log \left(\frac{4mn}{\epsilon} \right) \right) \leq \epsilon.$$

That is, with probability at least $1 - \epsilon$, multiplying on both sides by a randomized Hadamard transform or a randomized FFT yields a weight matrix that is μ_W -incoherent, where

$$\mu_W = 2 \log \left(\frac{4mn}{\epsilon} \right).$$

Proof. From Lemma A.2,

$$\mathbf{P} \left(|b^T U S x| \geq \|b\| \|x\| \sqrt{\frac{2}{n}} \log \left(\frac{4mn}{\epsilon} \right) \right) \leq \frac{\epsilon}{2mn}.$$

By applying this once on each side to the rows and columns respectively, and union bounding over the mn entries, we get

$$\mathbf{P} \left(|e_i^T H_L S_L W S_R^T H_R^T e_j| \geq \|W\|_F \sqrt{\frac{4}{mn}} \log \left(\frac{4mn}{\epsilon} \right) \right) \leq \epsilon.$$

The proof in the FFT case is identical. □

Lemma 3.1. Let H be any positive semidefinite matrix on $\mathbb{R}^{n \times n}$ and W any weight matrix on $\mathbb{R}^{m \times n}$. Let $U \in \mathbb{R}^{m \times m}$ and $V \in \mathbb{R}^{n \times n}$ be orthogonal scaled Hadamard matrices. Let $S_U \in \mathbb{R}^{m \times m}$ and $S_V \in \mathbb{R}^{n \times n}$ be random diagonal matrices with independent diagonal elements drawn uniformly from $\{-1, +1\}$. Then for any $\delta > 0$, $V S_V H S_V V^T$ is μ_H -incoherent with probability at least $1 - \delta$, and $U S_U W S_V V^T$ is μ_W -incoherent with probability at least $1 - \delta$, where

$$\mu_H = \sqrt{2 \log \left(\frac{2n^2}{\delta} \right)} \quad \text{and} \quad \mu_W = 2 \log \left(\frac{4mn}{\delta} \right).$$

Proof. The incoherence of H follows from the application of Lemma A.3. The incoherence of W follows from the application of Lemma A.4. □

A.2. Incoherence Processing with the Randomized Fast Fourier Transform (RFFT)

Here we described the Randomized Fast Fourier Transform (RFFT), $x \rightarrow VSx$ where $V \in \mathbb{C}^{n/2 \times n/2}$ is the discrete Fourier transform matrix, $S \in \mathbb{C}^{n/2}$ is a random complex phase vector, and $x \in \mathbb{R}^n$. The discrete Fourier transform can be computed in $O(n \log n)$ time via the fast Fourier transform. Here it is understood that the FFT operates over the reals, in that a vector $x \in \mathbb{R}^n$ is mapped to a complex representation $\mathbb{C}^{n/2}$, the RFFT is performed, and the resulting vector mapped back to \mathbb{R}^n . Here the mapping simply represents reshaping real-valued x into dimension $(n/2, 2)$, and interpreting the corresponding 2-tuples as a complex number.

Incoherence processing via the RFFT achieves similar theoretical guarantees as the RHT, see Lemmas A.3 and A.4. Ultimately the choice of the orthogonal transformation is up to the user. A Fourier transform works almost as well as a Hamard transform in practice (Table 1), so if a fast Hadamard implementation is not available, the FFT is a good option.

B. Block LDLQ

Lemma B.1. *Let $H \in \mathbb{R}^{nd \times nd}$ be a positive definite matrix with d -block LDL decomposition $H = L^T DL$. Then*

$$\text{tr}(D) \leq \text{tr}\left(H^{1/2}\right) \cdot \left\|H^{1/2} \odot M_D\right\|_2,$$

where $M_D = I \otimes \mathbf{1}_{d \times d}$ is the block diagonal mask. If, in addition, H is μ -incoherent in the sense that its matrix of eigenvectors U has

$$\|U_{ij}\| \leq \frac{\mu}{\sqrt{nd}},$$

then

$$\text{tr}(D) \leq \frac{\mu^2}{n} \text{tr}\left(H^{1/2}\right)^2.$$

Proof. Consider the optimization problem

$$\begin{aligned} &\text{minimize: } \text{tr}(R^T H R) \\ &\text{subject to: } R \text{ unit block lower diagonal.} \end{aligned}$$

Observe that the derivative of the loss is

$$\nabla f(R) = HR.$$

If $R = L^{-1}$, then $HR = L^T D$. But this must be a block upper triangular matrix, because it's the product of a unit upper triangular matrix (L^T) and a block diagonal matrix D . It follows that $\nabla f(L^{-1})$ is zero in all the directions in which we could move R , since R only varies in the strictly lower triangular directions. Therefore, $R = L^{-1}$ is the solution to this optimization problem, and for any R , $\nabla f(R) \geq \nabla f(L^{-1}) = \text{tr}(D)$.

Now, let M denote the strictly block lower triangular mask, and observe that $M + M^T + M_D = \mathbf{1}_{nd \times nd}$. Set $\alpha = \left\|H^{1/2} \odot M_D\right\|_2^{-1}$, and consider $R = (I + \alpha M \odot H^{1/2})^{-1}$. Observe that

$$\begin{aligned} \left(I + \alpha M \odot H^{1/2}\right)^T \left(I + \alpha M \odot H^{1/2}\right) &= I + \alpha M \odot H^{1/2} + \alpha M^T \odot H^{1/2} + \alpha^2 (M^T \odot H^{1/2})(M \odot H^{1/2}) \\ &\succeq I + \alpha (M + M^T) \odot H^{1/2} \\ &\succeq \alpha M_D \odot H^{1/2} + \alpha (M + M^T) \odot H^{1/2} \\ &\succeq \alpha H^{1/2}. \end{aligned}$$

It follows by inverting both sides that $RR^T \preceq \alpha^{-1} H^{-1/2}$.

So, for this R ,

$$\text{tr}(R^T H R) = \text{tr}(H R R^T) \leq \alpha^{-1} \text{tr}\left(H^{1/2}\right).$$

This proves the first part of the lemma. For the second part, observe that

$$\begin{aligned} \left\| H^{1/2} \odot M_D \right\|_2 &\leq \sum_{i=1}^{nd} \lambda_i^{1/2} \|(u_i u_i^T) \odot M_D\|_2 \\ &\leq \frac{\mu^2}{n} \operatorname{tr}(H^{1/2}). \end{aligned}$$

This proves the lemma. □

Theorem 4.1. *Suppose that we round $W \in \mathbb{R}^{m \times n}$ using g -block LDLQ with Hessian H , producing \hat{W} . Suppose that H is μ -incoherent, and that we use a (possibly stochastic) vector quantizer \mathbf{Q} that satisfies $\mathbf{E}[(\mathbf{Q}(x) - x)(\mathbf{Q}(x) - x)^T] \preceq \sigma^2 I$ for any $x \in \mathbb{R}^g$. Then*

$$\mathbf{E}[\operatorname{tr}((\hat{W} - W)H(\hat{W} - W)^T)] \leq \frac{gm\mu^2\sigma^2}{n} \operatorname{tr}(H^{1/2})^2.$$

Proof. First recall that from the description of block LDLQ,

$$\hat{W}_k = \mathbf{Q}(W_k + (W_{:(k-1)} - \hat{W}_{:(k-1)})\mathbf{A}_k).$$

We can also write this in matrix form in terms of the matrix \mathbf{L}_k as

$$\hat{W} = \mathbf{Q}(W + (W - \hat{W})(\mathbf{L}^T - I)).$$

Here, \mathbf{Q} is interpreted as operating independently block-wise. Let η denote the quantization error

$$\eta = (W + (W - \hat{W})(\mathbf{L}^T - I)) - \mathbf{Q}(W + (W - \hat{W})(\mathbf{L}^T - I)).$$

Then

$$\hat{W} = (W + (W - \hat{W})(\mathbf{L}^T - I)) - \eta,$$

which simplifies to

$$(W - \hat{W})\mathbf{L}^T = \eta.$$

This means that

$$\mathbf{E}[\operatorname{tr}((\hat{W} - W)H(\hat{W} - W)^T)] = \mathbf{E}[\operatorname{tr}((\hat{W} - W)\mathbf{L}^T \mathbf{D} \mathbf{L}(\hat{W} - W)^T)] = \mathbf{E}[\operatorname{tr}(\eta^T \mathbf{D} \eta)].$$

But by assumption, $\mathbf{E}[\eta\eta^T] \preceq m\sigma^2 I$ (since each block is just an independent application of \mathbf{Q} and we sum over m rows), so

$$\mathbf{E}[\operatorname{tr}((\hat{W} - W)H(\hat{W} - W)^T)] \leq m\sigma^2 \mathbf{E}[\operatorname{tr}(\mathbf{D})].$$

Combining this with the result of Lemma B.1 proves the theorem. □

C. E8P details

C.1. Constructing S

We use the following 29 elements of \hat{D}_8 with norm squared 12 to pad S to 256 entries.

$$\begin{aligned} &([3, 1, 1, 1, 3, 3, 3, 3] [1, 3, 1, 1, 3, 3, 3, 3] [1, 1, 3, 1, 3, 3, 3, 3] \\ &[1, 1, 1, 3, 3, 3, 3, 3] [3, 3, 3, 1, 3, 3, 1, 1] [3, 3, 3, 1, 3, 1, 3, 1] \\ &[3, 3, 3, 1, 1, 3, 3, 1] [3, 3, 3, 1, 3, 1, 1, 3] [3, 3, 3, 1, 1, 3, 1, 3] \\ &[3, 3, 3, 1, 1, 1, 3, 3] [3, 3, 1, 3, 3, 3, 1, 1] [3, 3, 1, 3, 3, 1, 3, 1] \\ &[3, 3, 1, 3, 1, 3, 3, 1] [3, 3, 1, 3, 3, 1, 1, 3] [3, 3, 1, 3, 1, 3, 1, 3] \\ &[3, 3, 1, 3, 1, 1, 3, 3] [3, 1, 3, 3, 3, 3, 1, 1] [3, 1, 3, 3, 3, 1, 3, 1] \\ &[3, 1, 3, 3, 1, 3, 3, 1] [3, 1, 3, 3, 3, 1, 1, 3] [3, 1, 3, 3, 1, 3, 1, 3] \\ &[1, 3, 3, 3, 1, 1, 3, 3] [1, 3, 3, 3, 3, 3, 1, 1] [1, 3, 3, 3, 3, 1, 3, 1] \\ &[1, 3, 3, 3, 1, 3, 3, 1] [1, 3, 3, 3, 3, 1, 1, 3] [1, 3, 3, 3, 1, 3, 1, 3] \\ &[1, 1, 3, 3, 1, 3, 3, 3] [3, 3, 1, 1, 3, 3, 3, 1]) / 2 \end{aligned}$$

C.2. Example Decoding with E8P

Here, we give an example of decoding with E8P. In this example, the first 8 bits of the codeword encode the entry in S , the next 7 bits encode the 7 right sign flips, and the last bit encodes whether or not we shift by $\frac{1}{4}$. Let the codeword be 0001010110010111. The first 8 bits 00010101 = 21 would indicate that we start with the 21st entry in S . In this example, let that be the vector

$$s = \left\{ \frac{1}{2}, \frac{1}{2}, \frac{1}{2}, \frac{3}{2}, \frac{1}{2}, \frac{1}{2}, \frac{1}{2}, \frac{1}{2} \right\},$$

which is not in \hat{D}_8 . Thus, s requires an odd number of sign flips to get into \hat{D}_8 . Then, the next 7 bits 1001011 would indicate that we need to negate the 1st, 2nd, 4th, and 7th from right bits. Since we need an odd number of sign flips, the 8th from right bit is also a sign flip. The sign-decoded vector is then

$$\left\{ -\frac{1}{2}, -\frac{1}{2}, \frac{1}{2}, \frac{3}{2}, -\frac{1}{2}, \frac{1}{2}, -\frac{1}{2}, -\frac{1}{2} \right\},$$

which we can verify is in E_8 . Finally, the last bit 1 indicates that we need to add $\frac{1}{4}$, so the final decoded vector is

$$\left\{ -\frac{1}{4}, -\frac{3}{4}, \frac{3}{4}, \frac{7}{4}, -\frac{1}{4}, \frac{3}{4}, -\frac{1}{4}, -\frac{1}{4} \right\},$$

which is in $E_8 + \frac{1}{4}$ as desired.

C.3. Why not K-Means?

A significant motivating factor behind E8P is that post-incoherence processing, entries of W are approximately Gaussian distributed. However, E8P is uniformly distributed, which raises the question: why not use a K-means based codebook? K-means based codebooks offer strong theoretical performance but have a few issues. First, it is difficult to enforce symmetry in a “learned” K-means codebook. This is crucial to be able to have a compressible codebook. If we force sign symmetry by learning cluster centers on only the positive orthant of a n -dimensional Gaussian, we can get around this but sacrifice accuracy at the axis region. Second, using K-means requires storing a codebook in fp16, whereas the entries of E8P can be stored as 4 bit integers. This means that during inference, the source codebook for a 8 dimension K-means codebook will be 4 times larger than the source codebook of E8P, running the risk of a cache eviction. Finally, we observe that empirically, E8P actually *outperforms* K-means, which is somewhat interesting and suggests that allocating more information to the edge of the distribution, even after incoherence processing, is useful.

D. Fine-Tuning During Quantization

In Algorithm 5 we describe our fine tuning procedure for QuIP#.

E. Additional Results

E.1. QuIP# on Mixtral 8x7B (Jiang et al., 2024) and Falcon 180B (Almazrouei et al., 2023)

Table 6. 2 bit QuIP# without fine-tuning on Mixtral 8x7B, a mixture of experts (MoE), and Falcon 180B, a non-Llama-based model. QuIP# scales to different architectures without issue.

MODEL	BITS	WIKI2	C4	ARCC	ARCE	BOOLQ	PIQA	WINO
MIXTRAL-8x7B	16	3.45	6.85	0.56	0.74	0.85	0.84	0.75
MIXTRAL-8x7B	2	4.69	8.25	0.49	0.68	0.81	0.80	0.73
FALCON-180B	16	3.30	6.31	0.61	0.82	0.87	0.85	0.81
FALCON-180B	2	4.18	7.06	0.58	0.81	0.84	0.84	0.81

Algorithm 5 QuIP# with Fine-Tuning

Require: Unquantized Model M , Development Set \mathcal{D} , Quantization Order O ,

Ensure: Quantized Model M

$X \leftarrow M_{\text{embedding}}(\mathcal{D})$

$C \leftarrow M(\mathcal{D})_{\text{logits}}$

for Decoder Block $D \in M$ **do**

$Y \leftarrow D(X)$

$X_{\text{train}}, Y_{\text{train}}, X_{\text{valid}}, Y_{\text{valid}} \leftarrow \text{split}(X, Y)$

for Linear Layer $L \in D$ in order specified by O **do**

$\hat{L} \leftarrow \text{QuIP\#-NoFT}(L)$

Disable gradients for the weight matrix (but not S_U, S_V) of \hat{L} .

Optimize D to minimize $\text{MSE}(D(X_{\text{train}}), Y_{\text{train}})$ using $X_{\text{valid}}, Y_{\text{valid}}$ for early stopping.

end for

$X \leftarrow Y$

end for

{At this point, the learnable parameters in M are the layernorms, all S_U and S_V , and the language model head.}

$\mathcal{D}_{\text{train}}, C_{\text{train}}, \mathcal{D}_{\text{valid}}, C_{\text{valid}} \leftarrow \text{split}(\mathcal{D}, C)$

Optimize M to minimize $\text{CrossEntropy}(M(\mathcal{D}_{\text{train}}), C_{\text{train}})$ using $\mathcal{D}_{\text{valid}}, C_{\text{valid}}$ for early stopping.

E.2. Zeroshot performance for ablation on lattice codebooks and fine-tuning

Table 7. Ablation on lattice codebooks and fine-tuning. QuIP# no FT and E_8 uses the RHT to perform incoherence processing but does not use lattice codebooks or fine-tuning. QuIP# No FT uses lattice codebooks but not fine-tuning. QuIP# uses lattice codebooks and performs fine-tuning.

MODEL	METHOD	BITS	ARCC (ACC_NORM)	ARCE (ACC_NORM)	BOOLQ (ACC)	PIQA (ACC_NORM)	WINO (ACC)
2-70	NATIVE	16	48.0	59.7	76.6	80.9	76.8
2-70	QUIP# NO FT & NO E_8	4	49.4	60.1	77.6	80.7	76.1
2-70	QUIP# NO FT	4	48.3	60.1	78.4	80.6	76.2
2-70	QUIP#	4	48.3	59.4	77.4	80.7	77.1
2-70	QUIP# NO FT & NO E_8	3	47.4	59.1	75.8	80.9	77.5
2-70	QUIP# NO FT	3	47.9	59.9	78.8	79.9	77.0
2-70	QUIP#	3	48.4	59.5	74.8	80.3	76.4
2-70	QUIP# NO FT & NO E_8	2	43.5	56.2	75.1	78.1	76.0
2-70	QUIP# NO FT	2	47.2	59.5	79.1	78.6	74.2
2-70	QUIP#	2	47.7	59.1	80.3	79.4	75.9
2-13	NATIVE	16	44.3	58.0	69.0	79.0	69.9
2-13	QUIP# NO FT & NO E_8	4	43.7	58.6	70.1	78.7	69.6
2-13	QUIP# NO FT	4	42.9	56.4	67.8	78.9	69.9
2-13	QUIP#	4	44.2	57.7	69.7	78.9	69.9
2-13	QUIP# NO FT & NO E_8	3	42.1	55.2	70.0	77.8	69.5
2-13	QUIP# NO FT	3	41.9	57.7	73.3	78.1	68.0
2-13	QUIP#	3	43.3	57.7	69.8	78.4	69.1
2-13	QUIP# NO FT & NO E_8	2	36.3	50.8	67.4	73.4	63.1
2-13	QUIP# NO FT	2	37.1	50.1	66.5	75.7	63.6
2-13	QUIP#	2	41.3	55.1	68.3	77.4	67.7
2-7	NATIVE	16	40.6	53.5	71.0	76.9	67.0
2-7	QUIP# NO FT & NO E_8	4	39.5	51.9	71.3	76.6	67.3
2-7	QUIP# NO FT	4	40.4	53.7	68.5	77.2	67.5
2-7	QUIP#	4	40.1	53.4	69.9	76.5	67.6
2-7	QUIP# NO FT & NO E_8	3	38.1	52.6	65.2	76.1	65.1
2-7	QUIP# NO FT	3	37.7	53.1	70.6	76.7	67.6
2-7	QUIP#	3	39.4	53.8	69.7	76.1	66.5
2-7	QUIP# NO FT & NO E_8	2	29.2	42.5	63.3	68.0	59.0
2-7	QUIP# NO FT	2	32.5	42.8	62.3	71.2	62.4
2-7	QUIP#	2	36.1	50.5	68.3	74.9	64.9

E.3. More Scaling Plots

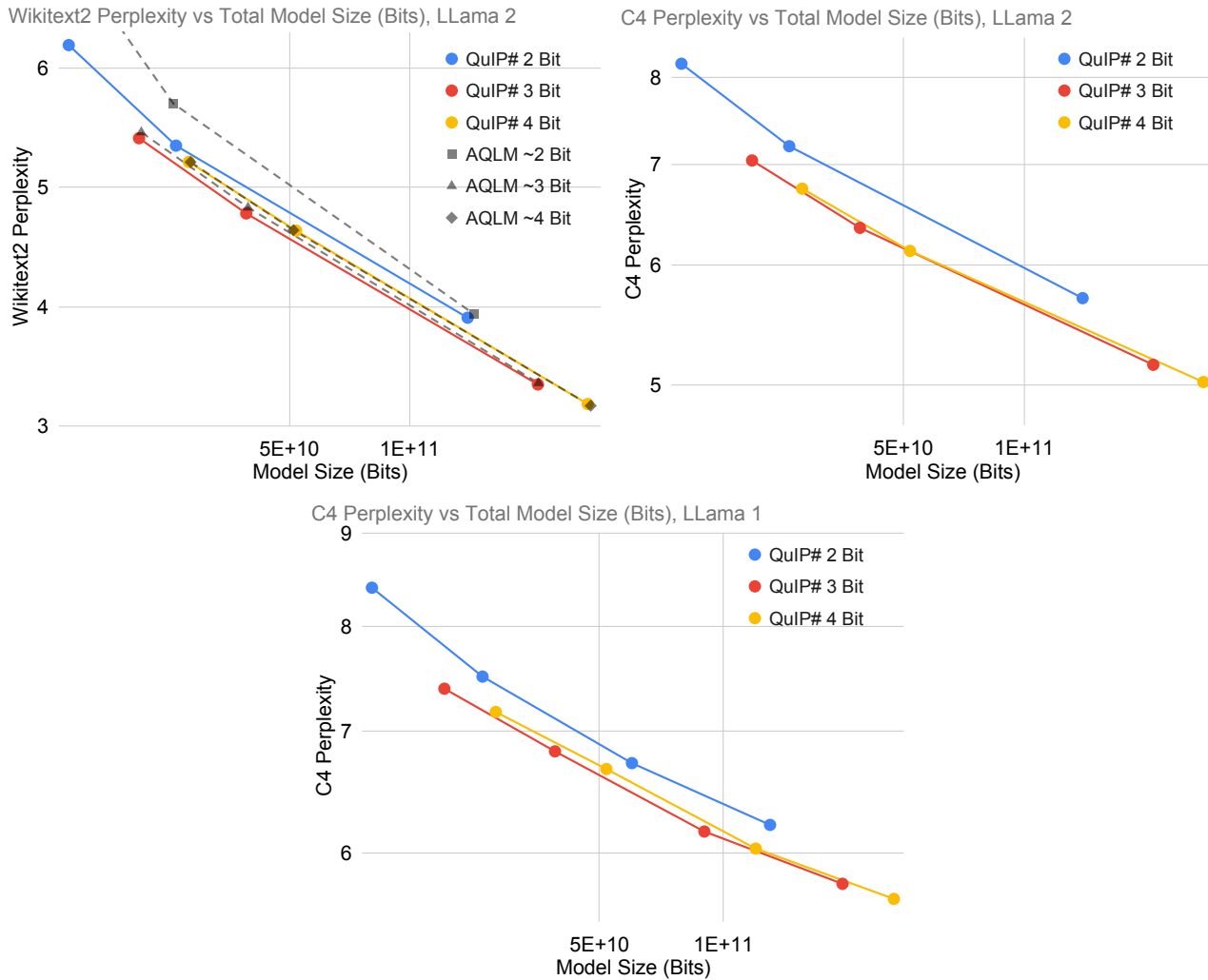


Figure 5. QuIP# scaling. (Top Left) Llama 2 Wikitext 2 perplexity vs AQLM. Context length 4096. QuIP# 2 and 3 bit scale better than AQLM 2 and 3 bit. (Top Right) Llama 2 C4 Perplexity. Context length 4096. (Bottom) Llama 1 C4 Perplexity. Context length 2048.

F. Implementation Details

This section contains implementation details for our Llama experiments. These details also mostly apply to the Mixtral and Falcon numbers except we use the Falcon dataset (Almazrouei et al., 2023) as it is publicly available.

F.1. Hessian Generation

Hessian matrices H were generated with 6144 sequences of a model’s native context length (2048 for Llama 1, 4096 for Llama 2) from the RedPajama 1T (Computer, 2023) dataset.

F.2. Hadamard Matrices

We use Hadamard matrices available at Neil Sloane’s website (Sloane).

F.3. Perplexity and Zeroshot Evaluation

We use the OPTQ (Frantar et al., 2023) “Wiktext2” and “C4” (not “C4 New”) sampling functions to calculate perplexity for our experiments. We use LM Eval (Gao et al., 2023) to calculate zeroshot numbers.

F.4. Fine Tuning

For the within-transformer block section of fine-tuning, we use the Adam optimizer (Kingma & Ba, 2017), a learning rate of 5×10^{-5} , batch size of 8, and sequence length equal to the model’s native context length. We train on small development dataset of 256 sequences from RedPajama 1T and validate on 128 sequences. We train for 5 epochs (160 steps) and keep the best model parameters based on the validation set. For the end to end tuning, we use the Adam optimizer, a learning rate of 5×10^{-5} , batch size of 1, sequence length equal to the model’s context length (except for 70B, where we had to use 3072 to avoid an OOM on our not very well optimized training script), and the same dataset and epoch setup as before. We observe that outside of using a low enough learning rate, the other hyperparameters did not affect fine-tuning much. For the 2 bit models, we used a learning rate of 5×10^{-4} for S_U and S_V (5×10^{-5} for everything else as above) for both the within-block and end to end fine tuning stages.

F.5. Hardware

All experiments were run on NVIDIA A100 GPUs except for the timing numbers, which were measured on a NVIDIA RTX 4090 to see what was possible with the current state-of-the-art NVIDIA consumer GPU. We find that we can quantize Llama 2 70B without fine tuning in under 10 GPU-hours and with fine tuning in around 100 GPU-hours. Both numbers do not include Hessian generation, which can be done once for a model and reused across many different quantization experiments.

F.6. Code and Prequantized Models

Our code is available at <https://github.com/Cornell-RelaxML/quip-sharp> and prequantized QuIP# models are available at <https://huggingface.co/relaxml>.

G. Example Generation

Below are some example generations from Llama 2 70B chat quantized with QuIP# to 2 bits, truncated to 256 tokens.

Prompt: How much wood could a woodchuck chuck if a woodchuck could chuck wood?

QuIP#:

The answer to this tongue-twister is a bit of a mystery. Woodchucks, also known as groundhogs, are rodents that burrow in the ground and are known for their ability to move large amounts of soil. However, there is no scientific evidence to suggest that they can actually chuck wood. The phrase “how much wood could a woodchuck chuck” was first used in a song called “The Woodchuck’s Song” in the late 19th century. The song was popularized by the singer and songwriter, Johnny Mercer, and it became a hit in the 1940s. The song’s lyrics include the line “How much wood could a woodchuck chuck if a woodchuck could chuck wood?” but they don’t provide an answer. In reality, woodchucks don’t chuck wood, they dig burrows. They are able to move a lot of soil and dirt as they dig their burrows, but they don’t have the ability to move wood. So, the answer to the tongue-

Prompt: Write a song about large language models to the tune of Mariah Carey's "All I Want For Christmas Is You"

QuIP#:

Verse 1:

I don't want a lot for Christmas
There's just one thing I'm wishing for
A language model that's large and bright
To help me with my writing, day and night

Chorus:

All I want for Christmas is a language model
A big, smart, AI that's my ideal
I'll be happy with just a few billion parameters
All I want for Christmas is a language model, yeah

Verse 2:

I'll be good, I won't be naughty
I'll use it for good, not for naughty
I'll generate text that's nice and neat
And make my writing life a treat

Chorus:

All I want for Christmas is a language model
A big, smart, AI that's my ideal
I'll be happy with just a few billion parameters
All I want for Christmas is a language model, yeah

Bridge:

I'

Prompt: Write some CUDA code that does a matrix multiply

QuIP#:

Here is a simple example of a matrix multiply using CUDA:

```
#include <cuda.h>
#include <cuda_runtime.h>

__global__ void matrixMultiply(float *A, float *B, float *C, int rowsA, int colsA, int rowsB, int colsB) {
    int i = blockIdx.x * blockDim.x + threadIdx.x;
    int j = blockIdx.y * blockDim.y + threadIdx.y;
    if (i < rowsA && j < colsB) {
        float sum = 0;
        for (int k = 0; k < rowsB; k++) {
            sum += A[i + k * colsA] * B[k + j * rowsB];
        }
        C[i + j * rowsB] = sum;
    }
}

int main() {
    int rowsA = 3;
    int colsA = 3;
    int rowsB = 3;
```